1-1-2015

Underlying scaling relationships between solar activity and geomagnetic activity revealed by multifractal analyses

Zu-Guo Yu

Vo Anh
University of Central Florida

Richard Eastes
University of Central Florida

AGU PUBLICATIONS

JGR

Journal of Geophysical Research: Space Physics

RESEARCH ARTICLE

10.1002/2014JA019893

Key Points:
- The scaling properties of the geomagnetic and the solar indices are examined
- The results suggest that multifractality exists in a_p, AE, Xl, and ion density
- The scaling similarity of the a_p and Xl data suggests flare-storm dependence

Correspondence to:
Z.-G. Yu,
yuzg1970@yahoo.com

Citation:
Yu, Z.-G., V. Anh, and R. Eastes (2014), Underlying scaling relationships between solar activity and geomagnetic activity revealed by multifractal analyses, *J. Geophys. Res. Space Physics*, *119*, 7577–7586, doi:10.1002/2014JA019893.

Received 18 FEB 2014
Accepted 30 AUG 2014
Accepted article online 2 SEP 2014
Published online 29 SEP 2014

Underlying scaling relationships between solar activity and geomagnetic activity revealed by multifractal analyses

Zu-Guo Yu[1,2], Vo Anh[2,3], and Richard Eastes[3]

[1]Hunan Key Laboratory for Computation and Simulation in Science and Engineering and Key Laboratory of Intelligent Computing and Information Processing of Ministry of Education, Xiangtan University, Xiangtan, Hunan, China, [2]School of Mathematical Sciences, Queensland University of Technology, Brisbane, Queensland, Australia, [3]Florida Space Institute, University of Central Florida, Orlando, Florida, USA

Abstract This paper identifies some scaling relationships between solar activity and geomagnetic activity. We examine the scaling properties of hourly data for two geomagnetic indices (a_p and *AE*), two solar indices (solar X-rays X_l and solar flux $F10.7$), and two inner heliospheric indices (ion density *Ni* and flow speed *Vs*) over the period 1995–2001 by the universal multifractal approach and the traditional multifractal analysis. We found that the universal multifractal model (UMM) provides a good fit to the empirical $K(q)$ and $\tau(q)$ curves of these time series. The estimated values of the Lévy index α in the UMM indicate that multifractality exists in the time series for a_p, *AE*, X_l, and *Ni*, while those for $F10.7$ and *Vs* are monofractal. The estimated values of the nonconservation parameter H of this model confirm that these time series are conservative which indicate that the mean value of the process is constant for varying resolution. Additionally, the multifractal $K(q)$ and $\tau(q)$ curves, and the estimated values of the sparseness parameter C_1 of the UMM indicate that there are three pairs of indices displaying similar scaling properties, namely a_p and X_l, *AE* and *Ni*, and $F10.7$ and *Vs*. The similarity in the scaling properties of pairs (a_p, X_l) and (*AE*, *Ni*) suggests that a_p and X_l, *AE* and *Ni* are better correlated—in terms of scaling—than previous thought, respectively. But our results still cannot be used to advance forecasting of a_p and *AE* by X_l and *Ni*, respectively, due to some reasons.

1. Introduction

Geomagnetic activity is sometimes quantified using indices including D_{st}, a_p, *AL*, and *AE* that measure the effects of the major current systems in the magnetosphere and ionosphere. On the other hand, solar activity is depicted in the solar irradiance (e.g., solar X-rays X_l and solar flux $F10.7$) and solar flares. Although the solar wind is known to be the primary source of energy that drives the dissipative processes in the magnetosphere, there still remain fundamental questions concerning how this energy is transformed into the various geomagnetic activity signatures [*Gleisner and Lundstedt*, 1997].

While D_{st} has been shown to be correlated with solar wind data [e.g., *Burton et al.*, 1975], the response of *AE* to the solar wind conditions has proved to be harder to determine [*Holzer and Slavin*, 1982; *Bargatze et al.*, 1985; *Vassiliadis*, 2006]. *Gleisner and Lundstedt* [1997] used solar wind density, velocity, and magnetic field as separate inputs into a neural network model to predict *AE*. They found that there exists influence of solar wind density, velocity, B_y, and B_z on the *AE* index, but the influence of B_x is not significant. The models proposed by *Li et al.* [2007] showed that the *AL* index is strongly dependent on the solar wind magnetic field and velocity but is practically independent of the solar wind density. Further, the *AE* model proposed by *Luo et al.* [2013] showed that solar flux $F10.7$ also plays a significant role in auroral activity.

Some researchers [*Gosling*, 1993; *Yermolaev et al.*, 2005; *Schwenn et al.*, 2005; *Zhang et al.*, 2007; *Yermolaev and Yermolaev*, 2009] reported that part of most major geomagnetic storms are caused by coronal mass ejections (CMEs). Solar active regions can produce CMEs with near-Sun speeds in excess of 900 km/s [e.g., *Sheeley et al.*, 1999] and solar flares. *Gopalswamy et al.* [2005] reported that part of the most energetic (X-class) flares are accompanied by fast CMEs. Based on the statistics from 103 events, *Howard and Tappin* [2005] found that approximately 40% of the X or M class flares were associated with observed shocks in the solar wind at Earth. Such shocks, which were attributed to CMEs, are a source of geomagnetic activity. *Yashiro et al.* [2005] collected 1301 X-ray flare events (above C3 level) detected by the GOES satellite and examined their CME associations using data from the Large Angle Spectrometric Coronagraph (LASCO).

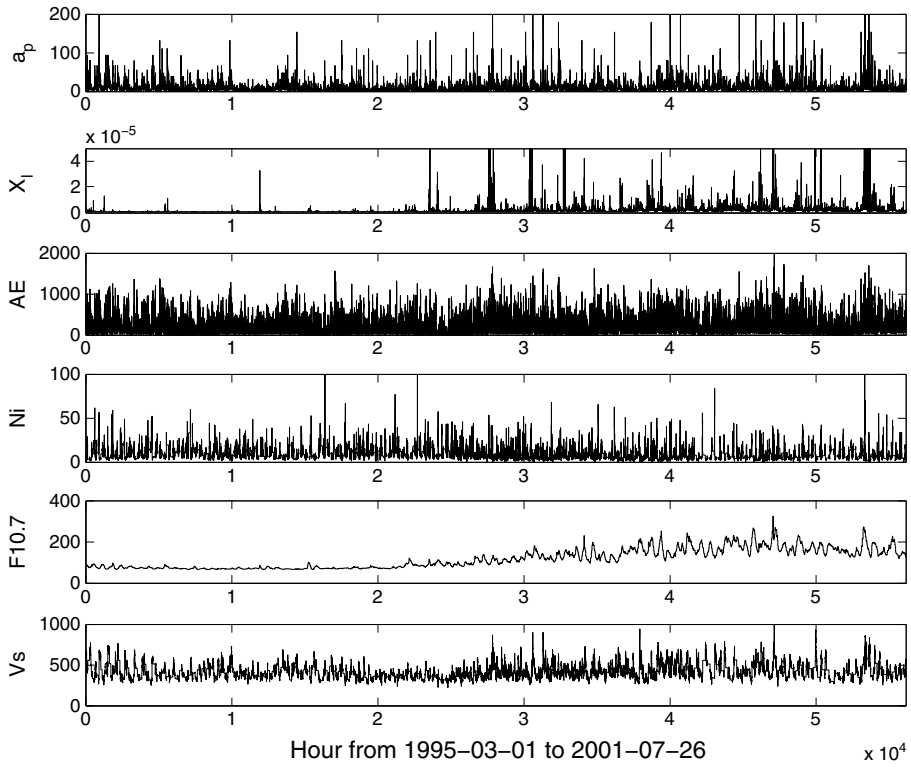

Figure 1. The hourly time series of the six indices from March 1995 to July 2001.

Their findings are (1) the CME association rate clearly increased with X-ray flare size from 20% for C-class flares (between C3 and C9 levels) to 100% for huge flares (above X3 level), (2) all CMEs associated with X-class flares were detected by the LASCO coronagraphs, while half (25–67%) of CMEs associated with C-class flares were invisible. *Yermolaev and Yermolaev* [2009] suggested that only a slight positive correlation between the classes of solar flare and geomagnetic storm occurrence is likely to be observed. *Yu et al.* [2009] investigated the flare-storm relation issue more rigorously using the tools of multifractal analysis (MFA).

In this paper, we continue to investigate the underlying scaling relationships between solar activity and geomagnetic activity. We expand the set of indices (1) a_p and *AE* for geomagnetic activity, (2) solar X-ray X_l and solar flux *F*10.7 for solar activity, and (3) ion density (*Ni*) and flow speed (*Vs*) of the inner heliosphere, which are solar wind parameters typically measured in situ at *L*1. In this work, we go beyond the second-order properties of these time series typically described by linear or nonlinear regressions. Our main tool is the scaling properties of time series.

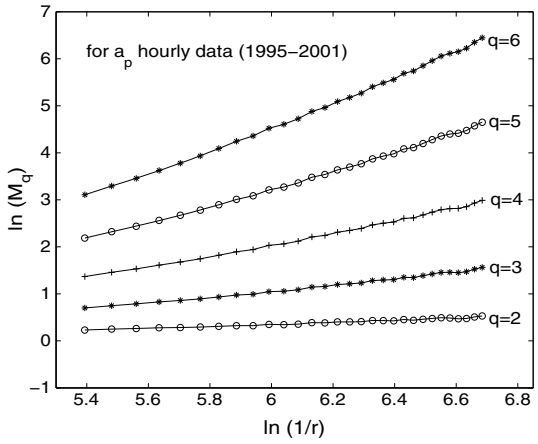

Figure 2. An example for obtaining the empirical $K(q)$ function.

These scaling properties have been characterized using fractal methods. Generalizing these methods, MFA has proved to be useful to characterize both theoretical and experimental heterogeneous spatial patterns [*Grassberger and Procaccia*, 1983; *Halsey et al.*, 1986]. MFA has been successfully applied in financial modeling [e.g., *Canessa*, 2000; *Anh et al.*, 2000], biological systems including DNA and protein sequences [e.g., *Anh et al.*, 2001, 2002; *Yu et al.*, 2001, 2003, 2004, 2006], and geophysical systems including rain and clouds

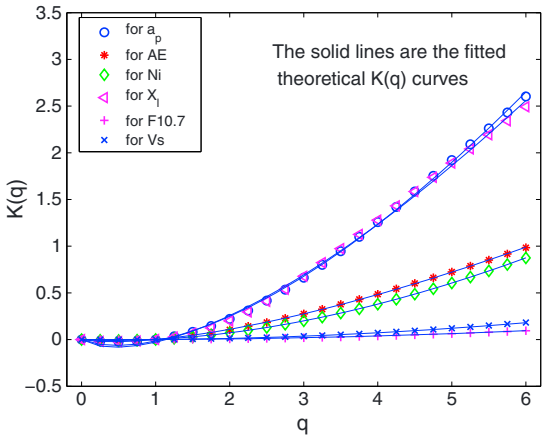

Figure 3. The $K(q)$ curves of the hourly data for the whole period (the curves indicated by symbols), and their fitted curves (solid lines) by the universal multifractal model.

[e.g., *Schertzer and Lovejoy*, 1987; *Schmitt et al.*, 1992; *Tessier et al.*, 1993, 1996; *Olsson and Niemzcynowicz*, 1996; *Harris et al.*, 1996; *Lovejoy et al.*, 1996, 2008; *Deidda*, 2000; *Lilley et al.*, 2006; *Kantelhardt et al.*, 2006; *Veneziano et al.*, 2006; *Venugopal et al.*, 2006; *Lovejoy and Schertzer*, 2006, 2010a, 2010b; *Garcia-Marin et al.*, 2008; *Serinaldi*, 2010; *Yu et al.*, 2014]. In particular, *Lui* [2002] successfully used fractal and multifractal approaches to extract salient features of the physical processes responsible for the near-Earth magnetospheric phenomena. *Abramenko* [2005] and *Georgoulis* [2012] analyzed multifractality of flaring active and quiet regions. *Wanliss et al.* [2005] provided a method to describe the multifractal property of the measure representation of the D_{st}. *Yu et al.* [2007] proposed a two-dimensional chaos game representation of the D_{st} index to predict geomagnetic storm events. *Yu et al.* [2009] used both multifractal detrended fluctuation analysis (MF-DFA) and traditional MFA to investigate the scaling properties of a_p, D_{st}, and the solar X-ray data. *Anh et al.* [2007, 2008] and *Yu et al.* [2010, 2012] used MFA and fractional stochastic differential equations to study the *AE* and geomagnetic field data.

This paper aims to identify significant similarities in the scaling properties of geomagnetic and solar indices. We use the universal multifractal approach [*Schertzer and Lovejoy*, 1987] and the traditional MFA to study the scaling properties of hourly data for a_p, *AE*, X_l, *F*10.7, *Ni*, and *Vs* over the period 1995–2001.

2. Data

The a_p index is a measure of the global changes in the geomagnetic field during a 3 h period. The eight a_p values for each day are based on the *K* index data from 11 Northern and 2 Southern Hemispheres magnetic observatories between the geomagnetic latitudes of 46° and 63°. Values of $a_p > 29$ are normally considered to indicate a geomagnetic storm, with a minor storm when $29 < a_p < 50$, a major storm when $50 \le a_p < 100$, and a severe storm when $a_p \ge 100$. The hourly interpolated a_p data were downloaded from the National Geophysical Data Center (NGDC, http://spidr.ngdc.noaa.gov/spidr/index.jsp). NGDC interpolated the 3-hourly a_p data into hourly data by setting the values of the following 2 h equal that of the current hour. (In fact, we tested that our results are not affected by different interpolations.)

The auroral electrojet (*AE*) index is derived from geomagnetic variations in the horizontal component observed at 12 observatories along the auroral zone in the Northern Hemisphere. The *AE* index then represents the geomagnetic (electrojet) activity in the auroral zone (see more details in *Anh et al.* [2008]). One-minute values of *AE* index are available from World Data Center-C2 for Geomagnetism in Kyoto (http://swdcdb.kugi.kyoto-u.ac.jp). The following analysis uses hourly averages of these 1 min values. The *AU* and *AL* indices were intended to express the strongest current intensity of the eastward and westward auroral electrojets, respectively.

Table 1. The Estimated Values of H, C_1, and α in the Universal Multifractal Model for the Hourly Data of the Six Indices (Whole Period)[a]

Data	H	C_1	α	Error
a_p	−0.0167	0.1777	1.3850	0.0151
X_l	−0.0270	0.2089	1.2081	0.0389
AE	0.0009	0.0711	1.2712	3.6546E-04
Ni	0.0012	0.0387	1.7406	2.4704E-06
*F*10.7	0.0004	0.0031	2.0000	3.7294E-06
Vs	0.0002	0.0060	1.9999	1.3492E-05

[a]Here *error* means the minimal value in equation (A4) of the Appendix A.

The solar X-ray data used in the analysis are from the GOES space environment monitor. Hourly data from GOES 6, 7, 8, 9, 10, 11, and 12 were downloaded from NGDC. X_l is observations with wavelength 1–8 Å.

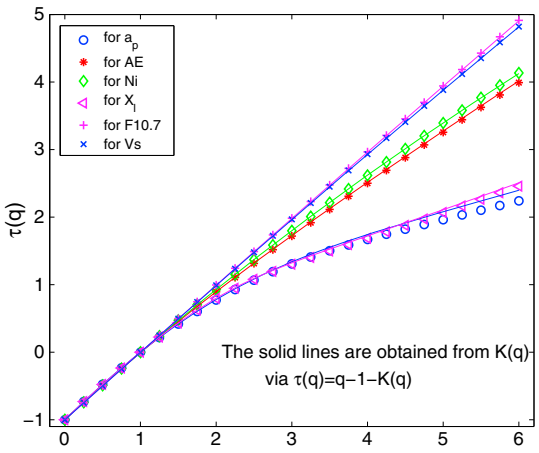

Figure 4. The $\tau(q)$ curves of the hourly data for the whole period (the curves indicated by symbols) and their fitted curves (solid lines) by the universal multifractal model.

Although any X-ray flare(s) associated with a CME event that produces a storm are observed at Earth 2–5 days earlier than the storm, there is evidence that ionospheric density changes caused by changes in the solar irradiance can persist for at least 3 days [*Wang et al.*, 2006].

The solar flux *F*10.7 index is a measure of the radiation from the Sun at wavelength of a 10.7 cm at the Earth's orbit. It is one of the most commonly used proxies for solar irradiance because it has a significant long-term correlation with X-ray, EUV, and UV fluxes from the Sun and with ionospheric and neutral densities in the upper atmosphere. Hourly *F*10.7 data were downloaded from NGDC.

Solar wind measurements, ion density (*Ni*) and flow speed (*Vs*), from the Wind satellite are included in the analysis. Hourly data were also downloaded from NGDC.

In this paper, we focus on the scaling property of the hourly data for geomagnetic indices a_p and *AE*, solar indices X_l and *F*10.7, and inner heliospheric indices *Ni* and *Vs*. Data from March 1995 through July 2001, which approximately cover the period from solar minimum to maximum, were used for this study. The last half of this period also overlaps with the January 1998 to August 2004 period used by *Howard and Tappin* [2005].

3. Results and Discussion

In the following, the scaling properties of the hourly data for a_p and *AE*, X_l and *F*10.7, *Ni*, and *Vs* will be examined by multifractal analyses. The observed data are shown in Figure 1.

First, we perform the MFA of the six series of data in Figure 1 via the universal multifractal model (UMM) (see the Appendix A for details of UMM). The empirical multifractal $K(q)$ functions are obtained from the slope of best linear fit of $\ln M_q(r_j)$ against $\ln(1/r_j)$ (the definitions of $K(q)$, $\ln M_q(r_j)$, and $\ln(1/r_j)$ are given in the Appendix A). We give an example to show how to obtain the $K(q)$ function in Figure 2. The resulting empirical $K(q)$ curves of these time series, for the whole period, are given in Figure 3 (the curves indicated by symbols).

Then we use the UMM (i.e., equation (A3) of the Appendix A) to fit the empirical $K(q)$ curves. The function *fminsearch* in MATLAB is used to solve the optimization problem (equation (A4) of the Appendix A) and

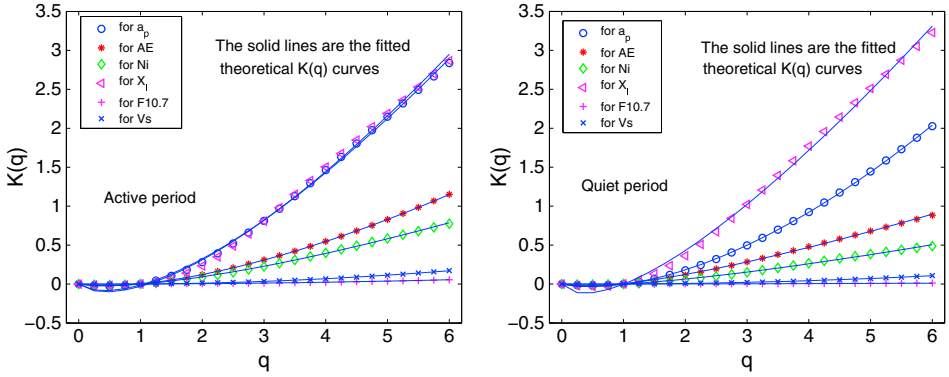

Figure 5. The $K(q)$ curves of the hourly data (the curves indicated by symbols) and their fitted curves (solid lines) by the universal multifractal model for the (left) active and (right) quiet periods.

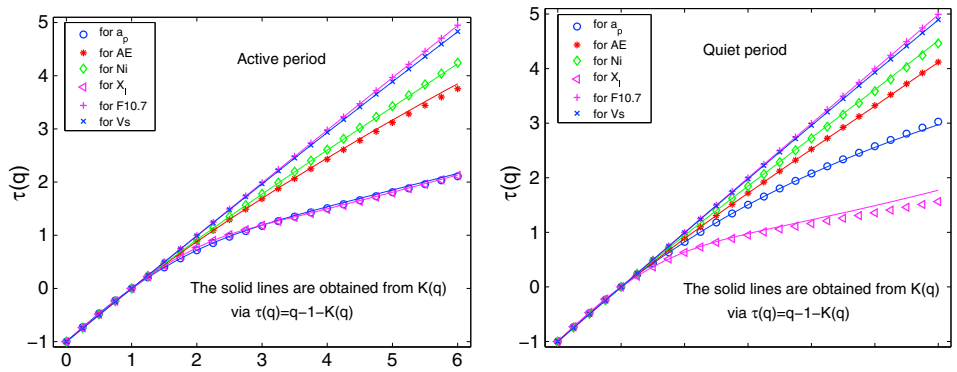

Figure 6. The $\tau(q)$ curves of the hourly data (the curves indicated by symbols) and their fitted curves (solid lines) by the universal multifractal model for the (left) active and (right) quiet periods.

estimate the values of three parameters H, C_1, and α of UMM (the initial values for these three parameters are set as 0.5, 0.5, and 1.5, respectively). In Table 1, we give the estimated values of these three parameters. The fitted $K(q)$ curves using the UMM are also given in Figure 3 (the solid lines). As seen in Figure 3, the UMM fits the empirical $K(q)$ curves very well. In Figure 3, three distinct groupings are evident: the $K(q)$ curve of a_p is almost identical with that of X_l, the $K(q)$ curve of *AE* is very close to that of *Ni*, and the $K(q)$ curves of *F*10.7 and *Vs* are very close to each other. This indicates that the three pairs a_p and X_l, *AE* and *Ni*, *F*10.7 and *Vs* share similar scaling properties, respectively.

The physical meaning of the three parameters H, C_1, and α of UMM can be found in the Appendix A. As seen in Table 1, the estimated values of α for a_p, X_l, *AE*, and *Ni* lie strictly in the range $(1, 2)$ for the whole period, indicating that the hourly data for these indices are multifractal. On the other hand, *F*10.7 and *Vs* have $\alpha = 2$, and their $K(q)$ curves shown in Figure 3 are flat, indicating that these two indices are monofractal depicted by the lognormal model. The estimated values of H in the UMM for the these time series almost equal to zero, indicating that these time series are conservative. The estimated values of the parameter C_1 exhibit the same grouping pattern as the $K(q)$ curves: a_p with X_l, *AE* with *Ni*, and *F*10.7 with *Vs*.

Since the time series are conservative, we can perform the traditional MFA (see the Appendix A for details). The empirical multifractal $\tau(q)$ functions are numerically estimated through a linear regression of $\ln Z_\epsilon(q)$ against $\ln \epsilon$ (the definitions of $\tau(q)$, $\ln Z_\epsilon q)$, and $\ln \epsilon$ are given in the Appendix A). In Figure 4 we show the empirical $\tau(q)$ curves of these time series for the whole period (the curves indicated by symbols). The $\tau(q)$ curves in Figure 4 have the same grouping pattern as the $K(q)$ curves.

We also use the UMM (with the same estimated parameters for $K(q)$) and equation (A9) of the Appendix A to fit the empirical $\tau(q)$ curves. The agreement between the fitted $\tau(q)$ curves (the solid lines) and the empirical curves shown in Figure 4 confirms that the UMM provides good fits to the empirical $\tau(q)$ curves.

From Figure 1, we also find that the pattern of X_l and *F*10.7 in almost the first half period, before $t = 22{,}000$ (hours from 1 March 1995 to the beginning of September 1998) differs from that in the second half period. The first and second half periods will be referred to as the quiet and active periods, respectively. As pointed out in *Yu et al.* [2009], conclusive results may not be obtained from data in the first half (quiet) period. However, the second half (active) period can be used to draw reliable, geophysical conclusions from the X-ray flare data X_l. Therefore, we performed the universal approach and traditional MFA on each period, active and quiet, separately. The $K(q)$

Table 2. The Estimated Values of H, C_1, and α in the Universal Multifractal Model for the Hourly Data of the Six Indices (Active Period)[a]

Data	H	C_1	α	Error
a_p	−0.0119	0.2369	1.1657	0.0259
X_l	−0.0294	0.2531	1.1518	0.0670
AE	0.0031	0.0727	1.3898	5.2400E-05
Ni	−0.0003	0.0644	1.1432	9.5809E-04
*F*10.7	0.0008	0.0017	2.0000	2.1190E-06
Vs	0.0001	0.0057	2.0000	1.9869E-05

[a]Here *error* means the minimal value in equation (A4) of the Appendix A.

Table 3. The Estimated Values of H, C_1, and α in the Universal Multifractal Model for the Hourly Data of the Six Indices (Quiet Period)[a]

Data	H	C_1	α	Error
a_p	−0.0026	0.1114	1.5569	9.8470E-04
X_l	−0.0016	0.3159	0.9751	0.0610
AE	0.0029	0.0861	0.9430	0.0015
Ni	−0.0013	0.0481	0.9912	0.0016
*F*10.7	0.0009	0.0001	2.5139	2.5606E-09
Vs	−0.0001	0.0036	2.0000	8.2657E-06

[a]Here *error* means the minimal value in equation (A4) of the Appendix A.

and $\tau(q)$ curves and their UMM fits are shown in Figures 5 and 6, respectively. The estimated values of the parameters in the UMM for the active and quiet periods are given in Tables 2 and 3, respectively. Again, the UMM can fit these $K(q)$ and $\tau(q)$ curves very well for both active and quiet periods. A marked difference is that the grouping pattern of a_p with X_l, *AE* with *Ni*, and *F*10.7 with *Vs* is pronounced for the active period; but this grouping is not conclusive, due to the reasons discussed above, for the quiet period.

The multifractal curves of a_p and X_l and *AE* and *Ni* are almost identical during the (active) times, respectively. This suggests that a_p and X_l, and *AE* and *Ni* are better correlated—in terms of scaling—than previous thought, respectively. Such a relationship is consistent with *Howard and Tappin*'s [2005] result which established an association between large solar flares and strong geomagnetic storms. Such a geomagnetic response is also consistent with increases in ionospheric electron density *Ni* and changes in the conductivity produced by X-ray radiation in flares [e.g., *Handzo et al.*, 2013] and the persistence over several days of electron density enhancements produced by solar irradiance changes [*Wang et al.*, 2006]. Indeed, part of the strongest geomagnetic storms are primarily caused by CMEs [*Gosling*, 1993; *Yermolaev et al.*, 2005; *Schwenn et al.*, 2005; *Zhang et al.*, 2007; *Yermolaev and Yermolaev*, 2009]; larger flares may indicate faster, hence statistically more geoeffective, CMEs. Solar active regions produce CMEs with near-Sun speeds around or excess of 900 km/s [e.g., *Sheeley et al.*, 1999] as well as solar flares. *Gopalswamy et al.* [2005] reported that part of the most energetic (X-class) flares are associated with fast CMEs. Hence, large flares (X-class) correlate to the fast CMEs, which cause the large geomagnetic storms. Therefore, our result is another confirmation of previously reported and widely known findings.

We also used the function *corr* in MATLAB to calculate the pairwise linear correlation coefficient between all indices using hourly data for the active period. The coefficients are given in Table 4. There are differences between the results from correlation analyses and those from multifractal analyses. We see that the correlation between a_p and *AE* is significant (up to 0.6377); *Vs* has positive correlation with *ap*, *AE*, and *F*10.7, while negative correlation with *Ni*; a_p and *AE* have almost no correlation with X_l; X_l has some positive correlation with *F*10.7, but no correlation with *AE*, a_p, *Ni*, and *Vs*. Prediction models of the geomagnetic *AL* and *AE* indices also showed significant relationships with *Vs* rather than *Ni* [*Li et al.*, 2007; *Luo et al.*, 2013]. However, the multifractal curves of *AE*, *Vs*, and *Ni* indicate that *AE* may actually have a more significant scaling correlation with *Ni* than with *Vs*. Multifractal analyses can detect higher-order non-Gaussian features in the data, while correlation analyses can only trace out second-order properties. Since correlation coefficients are sensitive to shifts in the time registration of the series being compared, irregularities in the time difference between the photon propagation times and parameters influencing geomagnetic activity, such as solar wind or orientation of the Earth, would result in the correlation being primarily an indicator of the longer-term (lower frequency) behavior of the series. The MFA is less sensitive to irregularities in the time shift and suggests that ion density may play a more significant role than has been previously identified.

Table 4. The Coefficients Between All Six Indices Using the Active Period Hourly Data

	a_p	X_l	*AE*	*Ni*	*F*10.7	*Vs*
a_p	1.0	0.0334	0.6377	0.1664	0.1115	0.3849
X_l	0.0334	1.0	0.0283	−0.0317	0.1898	0.0747
AE	0.6377	0.0283	1.0	0.0678	0.0990	0.3521
Ni	0.1664	−0.0317	0.0678	1.0	−0.1765	−0.2938
*F*10.7	0.1115	0.1898	0.0990	−0.1765	1.0	0.2681
Vs	0.3849	0.0747	0.3521	−0.2938	0.2681	1.0

In complex systems, scaling properties become relevant for understanding the interplay among various physical phenomena. Sometimes, relatively simple scaling laws, applicable to very complex systems, can provide clues to some fundamental aspects of the system. Thus, scaling properties are useful in understanding the basic physical principles involved in the Sun-Earth system.

4. Conclusions

The scaling properties of hourly data for the geomagnetic indices a_p and *AE*, and the solar indices solar X-ray X_l and solar flux *F*10.7, inner heliospheric indices ion density *Ni* and flow speed *Vs* during 1995 to 2001 period are examined by the universal multifractal approach and the traditional multifractal analysis. The numerical results from these multifractal analyses show that multifractality exists in the time series for a_p, *AE*, X_l, and *Ni*, while those for *F*10.7 and *Vs* are monofractal. We found that the universal multifractal model (UMM) can be used to fit the empirical multifractal $K(q)$ and $\tau(q)$ curves of these time series. The values of the Lévy index α in the UMM estimated also indicate that multifractality exists in a_p, *AE*, X_l, and *Ni* data. The values of nonconservation parameter *H* in the UMM estimated show that these time series are conservative which indicates that the mean value of the process is constant for varying resolution.

The multifractal $K(q)$ and $\tau(q)$ curves and the estimated values of the sparseness parameter C_1 in the UMM confirm that three pairs of data: a_p and X_l, *AE* and *Ni*, and *F*10.7 and *Vs* share similar scaling properties throughout the period examined, respectively. These results provide evidence that (1) the *AE* geomagnetic index may be more dependent on solar wind density than has been previously recognized and (2) the a_p index has a strong scaling correlation with changes in the solar X-rays. But our results still cannot be used to advance forecasting of a_p and *AE* by X_l and *Ni*, respectively, due to some reasons such as time shifts.

Appendix A: Multifractal Analyses

A1. Universal Multifractal Approach

Let $F(\xi)$ be a positive stationary stochastic process (cascade) on a bounded interval of the real field **R**, assumed to be the unit interval (0, 1) for simplicity, with expectation $E(F(\xi))=1$. The smoothing of $F(\xi)$ at scale $r>0$ is defined as $F_r(\xi)=\frac{1}{r}\int_{\xi-r/2}^{\xi+r/2} F(s)ds$. We consider the processes $X_r(\xi)=\frac{F_r(\xi)}{F_1(\xi)}$, $\xi \in [0,1]$. The multifractal function $K(q)$ is defined empirically (denoted as $K_d(q)$) as the power exponents if [*Anh et al.*, 2001]

$$E(X_r^q(\xi)) \propto r^{-K(q)}, \quad q \geq 0. \tag{A1}$$

The shape of the $K(q)$ curve can be used to determine whether a data set is monofractal or multifractal (a straight line indicates monofractal, a convex curve indicates multifractal) [e.g., *Garcia-Marin et al.*, 2008]. We will consider smoothing at discrete scales $0 < r_j < 1, j = 1, 2, \cdots$. Then from equation (A1), the $K(q)$ function for the data can be obtained by [*Anh et al.*, 2001]

$$K_d(q) = \lim_{j\to\infty} \frac{\ln X_{r_j}^q(\xi)}{-\ln r_j}. \tag{A2}$$

In practice, for a nonnegative time series $T(t)$, $t=1, 2, \ldots, N$, we can normalize it and define a measure μ in the following way. First, we define $F(t)=\frac{T(t)}{\sum_{i=1}^{N} T(i)}$ to be the frequency of $T(t)$, and $x(t)=\frac{t-1}{N}+\frac{1}{2N}$ (also normalizing the x coordinate to [0,1]). It follows that $\sum_{t=1}^{N} F(t) = 1$. Then for scale $0 < r_j < 1, j = 1, 2, \cdots$ and moment order $q \geq 0$, we define $Y_{r_j}(t)=\frac{1}{r_j}\sum_{(x(t)-r_j/2)\leq x(s)<(x(t)+r_j/2)} F(s)$ and $M_q(r_j)=\frac{1}{N}\sum_{t=1}^{N}[Y_{r_j}(t)]^q$. Then the empirical multifractal $K(q)$ function can be obtained from the slope of best linear fit of $\ln M_q(r_j)$ against $\ln(1/r_j)$.

In scaling processes, a scale invariant mechanism repeats scale after scale. A generic model, first studied in turbulence, is the cascade process [*Lovejoy et al.*, 2008]. In the past three decades, there has been an increasing interest in multifractals and the multiplicative cascade, which is a generic multifractal process [*Lovejoy and Schertzer*, 2010a]. Cascade processes generically lead to multifractal fields and have been used for simulating turbulent systems , including clouds, rain, temperature, wind, and passive scalars, as well as for solid Earth fields [*Lovejoy and Schertzer*, 2010a]. *Schertzer and Lovejoy* [1987] proposed the universal multifractal model (UMM) which assumes that the generator of multifractals is not only infinitely divisible but also has a

tractable Lévy stable distribution. In the framework of the UMM, the theoretical scaling exponent function $K(q)$ for the moments $q \geq 0$ of a cascade process [*Schertzer and Lovejoy*, 1987; *Ratti et al.*, 1994; *Garcia-Marin et al.*, 2008; *Serinaldi*, 2010] is given by

$$K(q) = qH + \begin{cases} C_1(q^\alpha - q)/(\alpha - 1), & \alpha \neq 1, \\ C_1 q \log(q), & \alpha = 1. \end{cases} \tag{A3}$$

Here the Lévy index $\alpha \in [0, 2]$ is the most significant parameter; it indicates the degree of multifractality. The value $\alpha = 0$ corresponds to the beta model, and $\alpha = 2$ corresponds to lognormal model. The beta model, also called beta-binomial model, and the lognormal model probably are multiplicative cascades characterized by the beta distribution and the lognormal distribution, respectively. The parameter H is the nonconservation parameter. A conservative process ($H = 0$) is defined when the mean value of the process is constant for varying resolution; while for a nonconservative process ($H \neq 0$), the mean value changes with the resolution [e.g., *Ratti et al.*, 1994; *Serinaldi*, 2010]. In our case, $C_1 \in [0, 1]$ describes the sparseness or inhomogeneity of the mean of the process [*Garcia-Marin et al.*, 2008].

Although the double trace moment technique [e.g., *Schmitt et al.*, 1992] has been widely used to estimate the parameters H, C_1, and α in geophysical research, it is complicated and the fitting of $K(q)$ is sometimes unsatisfactory [e.g., *Olsson and Niemczynowicz*, 1996; *Garcia-Marin et al.*, 2008; *Serinaldi*, 2010]. *Yu et al.* [2012] proposed a simple method to estimate the parameters H, C_1, and α. In this paper, we adopt the method in *Yu et al.* [2012]: If $K_T(q)$ represents the $K(q)$ function defined analytically by equation (A3) and $K_d(q)$ represents the $K(q)$ function obtained empirically, we can estimate the parameters by solving the least squares optimization problem

$$\min_{H, C_1, \alpha} \sum_{j=1}^{J} \left[K_T(q_j) - K_d(q_j)\right]^2. \tag{A4}$$

A2. Traditional Multifractal Analysis

The fixed-size box-counting algorithms is the most common algorithms of traditional MFA [*Halsey et al.*, 1986]. For a given measure ν with support A in one dimensional space $\mathbf{R}$, the partition sum is defined

$$Z_\epsilon(q) = \sum_{\nu(B)\neq 0} [\nu(B)]^q, \tag{A5}$$

$q \in \mathbf{R}$, where the sum is calculated overall different nonempty boxes $B = [k\epsilon, (k+1)\epsilon)$ of a given side ϵ in a grid covering of the support A. If

$$\tau(q) = \lim_{\epsilon \to 0} \frac{\ln Z_\epsilon(q)}{\ln \epsilon}. \tag{A6}$$

Then $\tau(q)$ is called the power law exponent of $Z_\epsilon(q)$. We denote $Z_{1,\epsilon} = \sum_{\nu(B)\neq 0} \nu(B) \ln \nu(B)$. Further, the generalized fractal dimensions of the measure are defined as

$$D(q) = \tau(q)/(q-1), \quad \text{for } q \neq 1, \tag{A7}$$

and

$$D(q) = \lim_{\epsilon \to 0} \frac{Z_{1,\epsilon}}{\ln \epsilon}, \quad \text{for } q = 1. \tag{A8}$$

The exponent $\tau(q)$ can be numerically estimated through a linear regression of $\ln Z_\epsilon(q)$ against $\ln \epsilon$.

The relationship between $\tau(q)$ and $K(q)$ pointed out by *Lovejoy et al.* [2008] is

$$\tau(q) = (q-1) - K(q), \tag{A9}$$

for one-dimensional data.

Acknowledgments

We wish to thank the Reviewers for their insights, comments, and numerous suggestions to improve the paper. We thank K.W. Ogilvie and A.J. Lazarus for the WIND data. This project was partially supported by the National Science Foundation of USA (NSF grant 0850396), the Natural Science Foundation of China (grant 11371016), the Chinese Program for Changjiang Scholars and Innovative Research Team in University (PCSIRT) (grant IRT1179), the Research Foundation of Education Commission of Hunan province of China (grant 11A122), and the Lotus Scholars Program of Hunan province of China.

Yuming Wang thanks the reviewers for their assistance in evaluating the paper.

References

Abramenko, V. I. (2005), Multifractal analysis of solar magnetograms, *Sol. Phys.*, *228*, 29–42.

Anh, V., K. S. Lau, and Z. G. Yu (2001), Multifractal characterisation of complete genomes, *J. Phys. A: Math. Gen.*, *34*(36), 7127–7139.

Anh, V. V., Q. M. Tieng, and Y. K. Tse (2000), Cointegration of stochastic multifractals with application to foreign exchange rates, *Int. Trans. Oper. Res.*, *7*, 349–363.

Anh, V. V., K. S. Lau, and Z. G. Yu (2002), Recognition of an organism from fragments of its complete genome, *Phys. Rev. E*, *66*, 031,910.
Anh, V. V., Z. G. Yu, and J. A. Wanliss (2007), Analysis of global geomagnetic variability, *Nonlinear Processes Geophys.*, *14*, 701–708.
Anh, V. V., J. M. Yong, and Z. G. Yu (2008), Stochastic modeling of the auroral electrojet index, *J. Geophys. Res.*, *113*, A10215, doi:10.1029/2007JA012851.
Bargatze, L. F., D. N. Baker, R. L. McPherron, and E. W. Hones (1985), Magnetospheric impulse response for many levels of geomagnetic activity, *J. Geophys. Res.*, *90*(A7), 6387–6394.
Burton, R. K., R. L. McPherron, and C. T. Russell (1975), An empirical relationship between interplanetary conditions and D_{st}, *J. Geophys. Res.*, *80*, 4204–4214.
Canessa, E. (2000), Multifractality in time series, *J. Phys. A: Math. Gen.*, *33*, 3637–3651.
Deidda, R. (2000), Rainfall downscaling in a space-time multifractal framework, *Water Resour. Res.*, *36*, 1779–1794.
Garcia-Marin, A. P., F. J. Jimenez-Hornero, and J. L. Ayuso-Munoz (2008), Universal multifractal description of an hourly rainfall time series from a location in southern Spain, *Atmosfera*, *21*(4), 347–355.
Georgoulis, M. K. (2012), Are solar active regions with major flares more fractal, multifractal, or turbulent than others?, *Solar Phys.*, *276*(1–2), 161–181.
Gleisner, H., and H. Lundstedt (1997), Response of the auroral electrojets to the solar wind modeled with neural networks, *J. Geophys. Res.*, *102*, 14,269–14,278.
Gopalswamy, N., S. Yashiro, Y. Liu, G. Michalek, A. Vourlidas, M. L. Kaiser, and R. A. Howard (2005), Coronal mass ejections and other extreme characteristics of the 2003 October–November solar eruptions, *J. Geophys. Res.*, *110*, A09S15, doi:10.1029/2004JA010958.
Gosling, T. T. (1993), The solar flare myth, *J. Geophys. Res.*, *98*, 18,937–18,949.
Grassberger, P., and I. Procaccia (1983), Characterization of strange attractors, *Phys. Rev. Lett.*, *50*, 346–349.
Halsey, T., M. Jensen, L. Kadanoff, I. Procaccia, and B. Schraiman (1986), Fractal measures and their singularities: The characterization of strange sets, *Phys. Rev. A*, *33*, 1141–1151.
Handzo, R., J. M. Forbes, and B. Reinisch (2013), Ionospheric electron density response to solar flares as viewed by digisondes, *Space Weather*, *12*(4), 205–216, doi:10.1002/2013SW001020.
Harris, D., M. Menabde, A. Alan Seed, and G. Geoff Austin (1996), Multifractal characterization of rain fields with a strong orographics influence, *J. Geophys. Res.*, *101*, 26,405–26,414.
Holzer, R. E., and J. A. Slavin (1982), An evaluation of three predictors of geomagnetic activity, *J. Geophys. Res.*, *87*, 2558–2562.
Howard, T. A., and S. J. Tappin (2005), Statistical survey of earthbound interplanetary shocks: Associated coronal mass ejections and their space weather consequence, *Astron. Astrophys.*, *440*, 373–383.
Kantelhardt, J. W., E. Koscielny-Bunde, D. Rybski, P. Braun, A. Bunde, and S. Havlin (2006), Long-term persistence and multifractality of precipitation and river runoff records, *J. Geophys. Res.*, *111*, D01106, doi:10.1029/2005JD005881.
Li, X., K. S. Oh, and M. Temerin (2007), Prediction of the *AL* index using solar wind parameters, *J. Geophys. Res.*, *112*, A06224, doi:10.1029/2006JA011918.
Lilley, M., S. Lovejoy, N. Desaulniers-Soucy, and D. Schertzer (2006), Multifractal large number of drops limit in rain, *J. Hydrol.*, *328*, 20–37.
Lovejoy, S., and D. Schertzer (2006), Multifractals, cloud radiances and rain, *J. Hydrol.*, *322*, 59–88.
Lovejoy, S., and D. Schertzer (2010a), On the simulation of continuous in scale universal multifractals. Part I: Spatially continuous processes, *Comput. Geosci.*, *36*, 1393–1403.
Lovejoy, S., and D. Schertzer (2010b), On the simulation of continuous in scale universal multifractals. Part II: Space-time processes and finite size corrections, *Comput. Geosci.*, *36*, 1404–1413.
Lovejoy, S., M. R. Duncan, and D. Schertzer (1996), Scalar multifractal radar observer's problem, *J. Geophys. Res.*, *101*, 26,479–26,491.
Lovejoy, S., D. Schertzer, and V. Allaire (2008), The remarkable wide range scaling of TRMM precipitation, *Atmos. Res.*, *90*, 10–32.
Lui, A. T. Y. (2002), Multiscale phenomena in the near-Earth magnetosphere, *J. Atmos. Sol. Terr. Phys.*, *64*, 125–143.
Luo, B., X. Li, M. Temerin, and S. Liu (2013), Prediction of the AU, AL, and AE indices using solar wind parameters, *J. Geophys. Res. Space Physics*, *118*, 7683–7694, doi:10.1002/2013JA019188.
Olsson, J., and J. Niemczynowicz (1996), Multifractal analysis of daily spatial rainfall distributions, *J. Hydrol.*, *187*(1–2), 29–43.
Ratti, S. P., G. Salvadori, G. Gianini, S. Lovejoy, and D. Schertzer (1994), Universal multifractal approach to internittency in high energy physics, *Z. Phys. C*, *61*, 229–237.
Schertzer, D., and S. Lovejoy (1987), Physical modeling and analysis of rain and clouds by anisotropic scaling of multiplicative processes, *J. Geophys. Res.*, *92*, 9693–9714.
Schmitt, F., D. Lavallee, D. Schertzer, and S. Lovejoy (1992), Empirical determination of universal multifractal exponents in turbulent velocity fields, *Phys. Rev. Lett.*, *68*, 305–308.
Schwenn, R., A. Dal Lago, E. Huttunen, and W. D. Gonzalez (2005), The association of coronal mass ejections with their effects near the Earth, *Ann. Geophys.*, *23*, 1033–1059.
Serinaldi, F. (2010), Multifractality, imperfect scaling and hydrological properties of rainfall time series simulated by continuous universal multifractal and discrete random cascade models, *Nonlinear Processes Geophys.*, *17*, 697–714.
Sheeley, N. R., J. H. Walters, Y.-M. Wang, and R. A. Howard (1999), Continuous tracking of coronal outflows: Two kinds of coronal mass ejections, *J. Geophy. Res.*, *104*(A11), 24,739–24,767.
Tessier, Y., S. Lovejoy, and D. Schertzer (1993), Universal multifractals: Theory and observations for rain and clouds, *J. Appl. Meteorol.*, *32*, 223–250.
Tessier, Y., S. Lovejoy, P. Hubert, D. Schertzer, and S. Pecknold (1996), Multifractal analysis and modeling of rainfall and river flows and scaling, causal transfer functions, *J. Geophys. Res.*, *101*, 26,427–26,440.
Vassiliadis, D. (2006), Systems theory for geospace plasma dynamics, *Rev. Geophys.*, *44*, RG2002, doi:10.1029/2004RG000161.
Veneziano, D., A. Langousis, and P. Furcolo (2006), Multifractality and rainfall extremes: A review, *Water Resour. Res.*, *42*, W06D15, doi:10.1029/2005WR004716.
Venugopal, V., S. G. Roux, E. Foufoula-Georgiou, and A. Arneodo (2006), Revisiting multifractality of high-resolution temporal rainfall using a wavelet-based formalism, *Water Resour. Res.*, *42*, W06D14, doi:10.1029/2005WR004489.
Wang, X., R. Eastes, S. WeicheckiVergara, S. Bailey, C. Valladares, and T. Woods (2006), On the short-term relationship between solar soft X-ray irradiances and equatorial total electron content (TEC), *J. Geophys. Res.*, *111*, A10S15, doi:10.1029/2005JA011488.
Wanliss, J. A., V. V. Anh, Z. G. Yu, and S. Watson (2005), Multifractal modelling of magnetic storms via symbolic dynamics analysis, *J. Geophys. Res.*, *110*, A08214, doi:10.1029/2004JA010996.
Yashiro, S., N. Gopalswamy, S. Akiyama, and G. Michalek (2005), Visibility of coronal mass ejections as a function of flare location and intensity, *J. Geophys. Res.*, *110*, A12S05, doi:10.1029/2005JA011151.

Yermolaev, Y. I., and M. Y. Yermolaev (2009), Does geomagnetic storm magnitude depend on solar flare importance?, *Cosmic Res.*, *47*, 460–465.

Yermolaev, Y. I., M. Y. Yermolaev, G. N. Zastenker, L. M. Zelenyi, A. A. Petrukovich, and J. A. Sauvaud (2005), Statistical studies of geomagnetic storm dependencies on solar and interplanetary events: A review, *Planet. Space Sci.*, *53*, 189–196.

Yu, Z. G., V. V. Anh, and K. S. Lau (2001), Measure representation and multifractal analysis of complete genomes, *Phys. Rev. E*, *64*, 031,903.

Yu, Z. G., V. Anh, and K. S. Lau (2003), Multifractal and correlation analysis of protein sequences from complete genome, *Phys. Rev. E*, *68*, 021,913.

Yu, Z. G., V. Anh, and K. S. Lau (2004), Chaos game representation of protein sequences based on the detailed HP model and their multifractal and correlation analyses, *J. Theor. Biol.*, *226*, 341–348.

Yu, Z. G., V. V. Anh, K. S. Lau, and L. Q. Zhou (2006), Fractal and multifractal analysis of hydrophobic free energies and solvent accessibilities in proteins, *Phys. Rev. E*, *63*, 031,920.

Yu, Z. G., V. V. Anh, J. A. Wanliss, and S. M. Watson (2007), Chaos game representation of the Dst index and prediction of geomagnetic storm events, *Chaos Soliton Fract.*, *31*, 736–746.

Yu, Z. G., V. Anh, and R. Eastes (2009), Multifractal analysis of geomagnetic storm and solar flare indices and their class dependence, *J. Geophys. Res.*, *114*, A05214, doi:10.1029/2008JA013854.

Yu, Z. G., V. Anh, Y. Wang, D. Mao, and J. Wanliss (2010), Modeling and simulation of the horizontal component of the geomagnetic field by fractional stochastic differential equations in conjunction with empirical mode decomposition, *J. Geophys. Res.*, *115*, A10219, doi:10.1029/2009JA015206.

Yu, Z. G., V. Anh, R. Eastes, and D. L. Wang (2012), Multifractal analysis of solar flare indices and their horizontal visibility graphs, *Nonlinear Processes Geophys.*, *19*, 657–669.

Yu, Z. G., Y. Leung, Y. D. Chen, Q. Zhang, and V. Anh (2014), Multifractal analyses of daily rainfall in the Pearl River basin of China, *Physica A*, *405*, 193–202.

Zhang, J., et al. (2007), Solar and interplanetary sources of major geomagnetic storms (Dst ≤ -100 nT) during 1996–2005, *J. Geophys. Res.*, *112*, A10102, doi:10.1029/2007JA012321.